19th IMEKO TC10 Conference
"MACRO meets NANO in Measurement for Diagnostics, Optimization and Control"
Delft, The Netherlands, September 21–22, 2023

Fine details of structural deviations in reference samples for scatterometry

Thomas Siefke[1,2], Lauryna Siaudinyté[2], Søren Alkærsig Jensen[3], Astrid Tranum Rømer[3], Poul-Erik Hansen[3]

[1]*Friedrich Schiller University Jena, Institute of Applied Physics, Jena, Germany,*
Thomas.Siefke@uni-jena.de
[2]*VSL Dutch Metrology Institute, Delft, Netherlands*
[3]*DFM - Danish National Metrology Institute, Hørsholm, Denmark*

***Abstract* – In order to fulfil Moore's law, the dimensions of the key elements of integrated circuits have been reduced to single digit nanometers. Besides enormous challenges for the micro- and nano fabrication methods itself, metrology is required for quality control to provide sub-nanometer uncertainties. Within the two EU founded projects ATMOC and POLight this challenge is tackled. In real world samples, deviations from the ideal geometries are encountered due to the complexities of fabrication processes. Understanding of these processes guides the development of procedures and helps in the reconstruction of the geometry from various scatterometric measurements. Here, we are reporting on the fabrication of reference samples for the mentioned projects and discuss the technological origins for such deviations.**

Keywords – Micro- and Nano fabrication, Deviation reference structures, Scatterometry, Industry, Innovation and Infrastructure

I. INTRODUCTION

Micro- and nanotechnology processes are providing the foundation of our modern world. Many products we are using in our everyday life are made using nanotechnology. This may be a microprocessor controlling a mobile phone or an extra-terrestrial rover, the PV-modules on a roof providing sustainable energy or a lab on a chip enabling a long and prosper life with a previously deadly disease. This process is fostered by Moore's law, which predicts a doubling of the number of transistors of an integrated circuit about every two years. This fast pace development leads to a so called "metrology gap" where the capabilities of the available metrology needed for process control lags behind. A promising class of methods to solve the issue is optical scatterometry.

Optical scatterometry is a class of methods where light with well-known properties is shone on a sample under investigation. From changes of the scattered light, various properties of the sample can be deduced via an inversion algorithm usually requiring *ab initio* knowledge about the structure. Scatterometry devices are usually very robust, non-destructive [1] and typically no constrains are imposed on the samples (compared to e.g. conductivity for CD-SEM) with an achievable uncertainty in the sub-nanometer range [2]. While the sensitivity to very fine sub-nanometer deviations of the structures is a major advantage of the method, it requires knowledge about fabrication technologies and the arising deviations from the metrologist. We aim to rise an awareness about distinctive deviations to help metrologists to make educated assumptions and guide them to more realistic models. As an example, we are presenting the fabrication of the reference structures and discussing the occurring deviations alongside.

II. LAYOUT OF REFERENCE SAMPLES

For the investigation, several reference samples were fabricated. In Figure 1 an example is shown. It consists of either a fused silica substrate or a silicon substrate where the structures are etched to a nominal height of 150 nm.

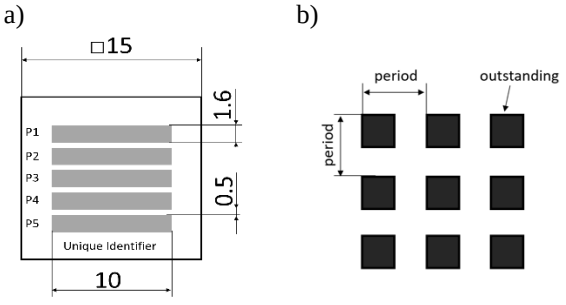

Figure 1: a) Layout of a reference chip. From these chips, 12 pieces are arranged on a 100 mm silicon wafer and b) schematic depiction of the nanostructures.

In the strip on the layout (Fig.1a) the period is varied according to table 1.

Table 1: Parameter variation with in the chip

Denotation	P1	P2	P3	P4	P5
Period / nm	43	326	438	589	1000

III. FABRICATION METHOD

For the fabrication of the samples, the respective substrates are first cleaned using an automatic wafer cleaner (SB30 OPTIwet) with Caro's acid, mega-sonic agitated water and high-pressure ammonia. Subsequently, the surface is etched for 15 s with an Ar-ion beam at 1300 eV in an Ionfab 300LC (OIPT) to remove any remaining surface contaminations such as silicon oxide and water. Next, 20 nm of chromium is deposited *in vacuo* by ion beam sputter deposition in the same tool from a square 250 mm 3N5 chromium target with Argon ions at 400 eV and 400 mA and additionally 2.5 sccm nitrogen flow. Afterwards, the samples are coated with an HMDS adhesion promoter in a Sawatec 200/300 for 60 s at 110°C after 10 min of dehydration at 150°C. Immediately afterwards, 100 nm of electron beam sensitive OEBR-CAN038 AE 2.0CP (Tokyo Ohka Kogyo Co. LTD) is applied by spin coating, and the pattern is generated using a Vistec 350OS electron beam writer with character projection apertures [3]. Subsequently, the structure is manually developed with OPD4262 for 30 s and thoroughly rinsed with DI water. The resist pattern is then transferred into the chromium layer by ion beam sputter etching at 1300 eV. Next, the remaining resist is stripped by 5 min oxygen plasma ashing and subsequently the pattern is transferred to a depth of 150 nm into the respective substrate by ICP etching in a SI500C (Sentech Instrumets GmbH). The actual recipe depends on the substrate and is fluorine based. Finally, the chromium is removed by manual wet etching with TechniEtch Cr01 (MicroChemicals GmbH).

In Figure 2 a) an SEM image of the resist pattern for a structure is shown. After the transfer into the substrate with the aforementioned process, the cross section of the structure is show in Figure 2 b).

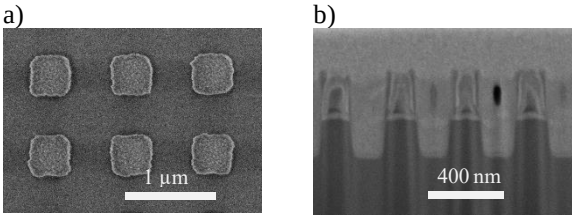

Figure 2 a) Top down SEM image of a resist structure and b) cross-section image of a structure prior to the hard mask removal. (Please note that the light grey layers are stemming from the FIB preparation for the cross-section image.)

It is notable, that the ridges show a side wall angle which is larger than 90° and exhibits varying degrees of rounding at the corners of the profile as well as in the top-down view. For a better understanding of the reasons, we will briefly recap the used processes in more detail and discuss the potential impact and pitfalls for optical scatterometric methods, regarding the shape and complex refractive index. Processes include:

- Deposition
- Electron beam lithography
- Etching

IV. DEVIATIONS

Deposition techniques, i.e., techniques to add a thin film of a certain material, are typically differentiated according to the state of the source material. This may be a liquid or a vapor solidifying on the substrate leaving the desired thin film.

In the process described, an example of the former is the *spin coating* of the e-beam sensitive resist. The measurement of resist thicknesses and profiles is an important task for process control. Such resists are often mixtures of a polymer matrix and various additives such as the photo-active component and solvents [6]. This regularly leads to distinctive features in the absorption, especially in the UV and FIR region. These features are prone to strong changes in shape or dimension, e.g. after drying of the solvent, rehydration, bleaching due to exposure, etc. This must be taken into account for a proper reconstruction. Furthermore, the resist may be unintentionally altered during the optical measurement.

Other examples of deposition processes include chemical vapor deposition (CVD) and physical vapor deposition (PVD). In CVD, gases are directly introduced and undergo a reaction (often initiated thermally or via a plasma) to produce the desired film. In PVD, a solid source material is first converted to vapor by heat or other physical interaction with photons or accelerated particles such as electrons or ions, etc. The material is then allowed to pass through a vacuum and condense onto the substrate. For further reading see [8]. The underlying physics of film formation is beyond the scope of this paper, but the layers obtained, in particular their complex refractive index, are usually very different from the bulk materials. This necessitated the separate determination of the refractive index for the deposition process under actual deposition conditions for our reference sample.

In the process described, *ion beam sputter deposition* is used to apply the chromium hard mask. This process utilizes argon ions from a broad (8 cm) ion beam source impinging on a 250 meV square chromium target. Due to the sputter process, particles with energies up to approximately 10 eV are released and condense at the sample surface. Due to the high particle energy, the film shows large grain sizes of several tens of nanometer. Since

this may have an effect on the line edge roughness of the future structures, there are additional 2.5 sccm of nitrogen introduced during deposition, hindering grain growth. Since the chromium layer serves as hard mask and is later removed, the refractive index was of no concern in this investigation.

Subsequent to the hard mask deposition, a resist mask is created by means of *electron beam lithography*. Upon local exposure to electrons, a resist is altered, making it selective to further chemical processing. The most common method is using a fine gaussian electron beam to pointwise expose the resist, enabling great resolution but rendering the method very slow. There are a variety of improvements to this method available, for the here demonstrated structures the most advanced cell projection e-beam lithography is used. For that purpose, a reticle is introduced into the electron beam optics, which contains apertures resembling a magnified portion of the desired geometry. Thereby, areas of several square micrometers are exposed in a single shot, reducing the writing time by two orders of magnitude. An area of 10 cm x 10 cm of the described structure can be exposed within approximately 6 h with the here shown process [3].

Looking at 3D structures such as arrays of rectangles, additional rounding of the corners becomes prominent. This stems from the back scattering of electrons from the substrate. The backscattered electrons can have a range of several micrometers and may cause blurring of the structure. This can be described by the convolution with a radially symmetric point spread function. For the 3D structures, several methods were applied to counteract this so-called proximity effect and receive the desired shapes.

Furthermore, the edges of all structures show a distinctive *line edge roughness* (standard deviation: 3.4 nm, correlation length: 15.3 nm and Hurst exponent: 1) [5] due to several effects such as shot noise of the electrons, random distribution of the electron sensitive molecules and random walk of the acid molecules during post exposure bake. In general, line edge roughness is difficult to handle in scatterometric measurements. Besides the high computational cost, the line edge roughness must be correctly resembled [5, 11]. However, it is both experimentally and analytically shown that the reconstructed line width is usually underestimated due to line edge roughness [4,5]. Especially for high refractive index materials, such as the silicon used here, this effect can be up to several nanometer. This renders the incorporation of LER crucial for sub-nanometer optical metrology.

Following the lithography, the pattern is transferred by *dry etching* into the underlying chromium and subsequently into the silicon substrate. The underlying mechanisms regarding etching are twofold. By bombardment with ions the lattice at the surface is damaged and may be sputtered, leading to a purely physical removal. A purely chemical removal can occur due to reactions with excited species, typically stemming from an etching gas in a plasma state. The first is mostly material unspecific and anisotropic, the latter shows a great selectivity between materials and isotropy. Often, a combination of both is employed to mitigate the advantages and disadvantages for the respective pattern transfer tasks.

In the example shown here, the chromium hard mask is patterned against the resist mask by *ion beam sputter etching*. For that, argon ions from an ion beam source (20 cm) are used. In the unprotected areas, the chromium is removed by sputtering. Parts of the removed material re-condensates at the side wall of the resist mask, forming an embankment, thereby stabilizing the edge of the hard mask against the later etching of the silicon substrate. This embankment can be seen in Fig. 2 b). Although this embankment can be very beneficial within the etching process, its geometry is rather complex. Further, the refractive index can vastly deviate from that of the closed layer due to the re-condensation and potential mixing with substrate material, rendering a scatterometric reconstruction extremely difficult. Next, the hard mask is transferred into the silicon substrate by means of *inductive coupled plasma etching*. For that, a water-cooled coil is used to supply energy into a gas to ignite and maintain a plasma. This gas is usually a mixture of several inert and reactive gases providing ions and reactive species, leading to a combination of physical and chemical removal processes. The material at the bottom of the unprotected areas is damaged or sputtered by impinging ions, increasing the reactivity with the excited species, leading to a good anisotropy. Further, gases containing fluorine, oxygen and carbon can lead to the formation and subsequent deposition of a polymer. Deposition and etching of this film are competing processes which are finely balanced in a dynamic equilibrium, leading to further protection of the sidewalls, while the substrate is always exposed at the bottom, further enhancing the anisotropy. If the equilibrium is slightly in favor of the polymer formation, the sidewall of the final structures shows a sidewall angle largen than 90°, i.e., their cross section resembles a trapezoid with a shorter top side. Additionally, sputter processes show a strong angle dependence resulting as well in positive sidewall angles, amplifying this effect. Furthermore, ions can be reflected at the sidewalls, depending on the actual conditions (angular spectra of incident ions, energies, angles, structure width) that can lead to a higher ion current at the bottom and thus a trench or rounding. The described effect leads to deviations of the actual structure from the desired ideal structure, making the required models for reconstruction more complex. Additionally, the surfaces may be altered, either due to remaining polymer, ion damage or oxidation. For sub-nanometer metrology this needs to be carefully considered.

V. SCATTEROMETRIC MEASUREMENTS

We performed Mueller ellipsometry measurements on the same two-dimensional grating structure of nominal pitch of 589 nm. In the experimental setup, which is described in detail in Ref. [9], we invoke photo-elastic modulators with 4 different angular settings to obtain all Mueller matrix elements except for the first one (m_{11}). We record the spectrum of the Mueller matrix elements for wavelengths in the range 250 nm to 850 nm. The beam size diameter is approximately 1 mm and the ellipsometry technique relies on the homogeneity of the sample within the illumination spot. By performing SEM measurements, we checked that the sample does indeed appear to be very homogeneous, see Fig. 4.

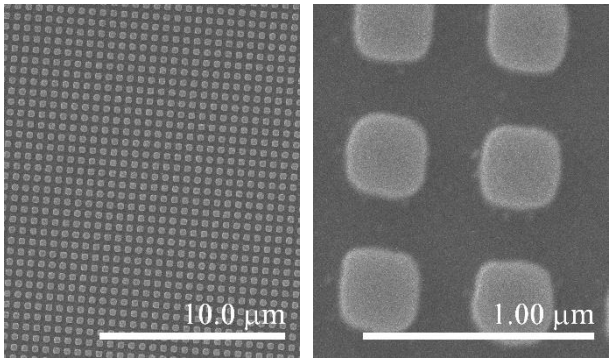

Figure 4: SEM pictures of nano pillars with pitch of 589 nm..

During the ellipsometry measurements, we aligned the sample with one of the grating axes in the scattering plane, in which case the Mueller matrix elements m_{13}, m_{14}, m_{23}, m_{24} as well as the symmetry-related partners m_{31}, m_{41}, m_{32}, m_{42} are expected to be zero. Through this procedure, we obtain the data shown in Fig. 5. As seen from the figure, the expected symmetries $m_{12}=m_{21}$, $m_{33}=m_{44}$, and $m_{34}=-m_{43}$ are clearly visible from the experimental data. At wavelength below 300 nm the data is more scattered. In this regime, we also find strong deviations from zero in the other Mueller matrix elements, which are expected to be zero for a square lattice in this alignment, as shown below in Fig. 7. We checked that this effect is due to the sample, as it was not present when scattering from a Si wafer. However, previously similar structures have been reported from a more rhombic arrangement of the pillars [10] and it could be speculated that a similar small rhombic deviation could give rise to these signatures.

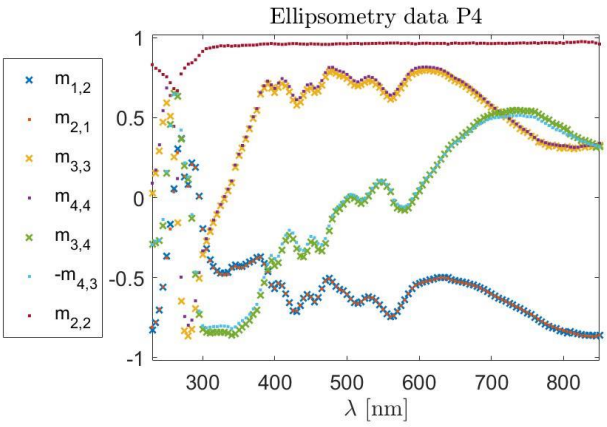

Figure 5: Measured ellipsometry spectrum for nano pillars with pitch of 589 nm in both directions.

VI. INVERSE MODELLING

To retrieve the structural parameters from the ellipsometry data, we calculate the reflection amplitudes of the two-dimensional square grid of pitch 589 nm in both directions. The pillars (see fig. 6) are modelled by height H and width W and the parameter R for a parametrization of the pillar cross section from circular to square. For $R = \frac{1}{\sqrt{2}}$ the pillars have a circular cross section of radius equal to half the pillar width. For $R = 1$, the pillars have a cross section which is square with the width given directly by W. In the intermediate cases, the corners are rounded and the radius of the associated circle is given by $R\frac{W}{\sqrt{2}}$.

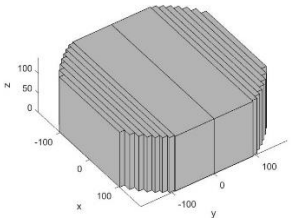

Figure 6: Cross section profile of a pillar with R=0.8.

We simulate the structures, keeping the refractive index fixed to that of Si in the (100) crystal orientation and comparing the experimental and simulated spectra in the wavelength regime of 350 nm – 850 nm. In this way, we omit the spectral region where additional features are present in the channels m_{13}, m_{14}, m_{23} and m_{24}, as discussed in the previous section.
From a library search, we found the best match between the measurement results and the simulated spectrum with the results stated in Table 2. It is seen that the best fit is found from rounded square structures with R=0.8.
Importantly, there is a strong correlation between the pillar width and the rounding parameter. This means that a different width is estimated if the rounding of the square

pillars is not taken into account in the inverse modelling. Specifically, we find for *R*=1.0 that the estimated width is 320 nm, instead of 340 nm as found for the corner-rounded pillars. On the other hand, the estimated height is 140 nm in both cases.

Table 2: Parameters from inverse modelling

Period / nm	Width / nm	Height / nm	*R*
Nominal	250	150	1.0
Ellipsometry	340	140	0.8

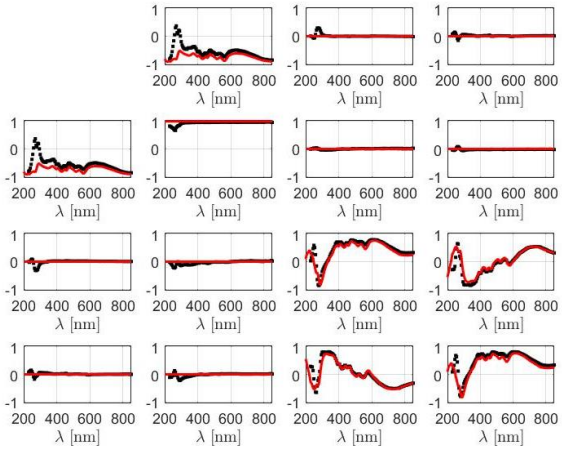

Figure 7: Ellipsometry data showing 15 Mueller matrix elements and the simulation curves of the best fit solution, see Table 2.

VII. CONCLUSIONS AND OUTLOOK

In this paper, we have discussed the fabrication of reference samples for nano-structured devices. According to the process chain shown, several such elements were fabricated and are subsequently investigated by SEM and scatterometry methods. Work on the reconstruction has been initiated.

VIII. ACKNOWLEDGMENTS

This project (20IND04 ATMOC and 20FUN02 POLight) has received funding from the EMPIR programme co-financed by the Participating States and from the European Union's Horizon 2020 research and innovation programme. This work is partly funded by The Danish Agency for Higher Education and Science.

REFERENCES

[1] **Madsen, M.H.; Hansen, P.E.**:Scatterometry—fast and robust measurements of nano-textured surfaces, *Surf. Topogr.: Metrol. Prop. 4 023003(2016)*

[2] **Siefke; T.; Hurtado, C.; Dickmann, J.; Dickmann, W.; Käseberg, T.; Meyer, J., Burger, S.; Zeitner,U.; Bodermann, B.; Kroker,S.**: *Quasi-bound states in the continuum for deep subwavelength structural information retrieval for DUV nano-optical polarizers,* Opt. Express 28, 23122-23132 (2020)

[3] **Hädrich, M., Siefke, T., Banasch, M. and Zeitner, U.D.**, Optical metasurfaces made by cell projection lithography. *PhotonicsViews,* 19, 28-31 (2022)

[4] **Thomas Siefke and Sebastian Heidenreich** "Systematic influence of line edge roughness on the line width measured by scatterometry", Proc. SPIE PC12619, Modeling Aspects in Optical Metrology IX, PC1261906 (23 August 2023); https://doi.org/10.1117/12.2675801

[5] **Thomas Siefke, Martin Heusinger, Carol B. Rojas Hurtado, Johannes Dickmann, Uwe Zeitner, Andreas Tünnermann, and Stefanie Kroker,** "Line-edge roughness as a challenge for high-performance wire grid polarizers in the far ultraviolet and beyond," Opt. Express 26, 19534-19547 (2018)

[6] **Chris Mack** "Fundamental Principles of Optical Lithography: The Science of Microfabrication" 978-0-470-72730-0 (2007)

[7] **Klaus Schuegraf** " Handbook of thin-film deposition processes and techniques", 0-8155-1153-1 (1988)

[8] **Ferreras Paz, V., Peterhänsel, S., Frenner, K.** *et al.* Solving the inverse grating problem by white light interference Fourier scatterometry. *Light Sci Appl* **1**, e36 (2012). https://doi.org/10.1038/lsa.2012.36

[9] **Hansen, P.-E., Johannsen, S. R., Jensen, S. A., and Madsen, J. S. M.**, "Enhanced measurement accuracy for nanostructures using hybrid metrology," Frontiers in Physics , 1–10 (2022).

[10]**Jana Grundmann, Tim Käseberg, Bernd Bodermann,** Optical measurements and numerical simulations of the Mueller matrix at silicon nanowire structures, SPIE (2023)

[11] **Chris A. Mack**, "Generating random rough edges, surfaces, and volumes," Appl. Opt. 52, 1472-1480 (2013)